

Collinear antiferromagnetic phases of a frustrated spin- $\frac{1}{2}$ J_1 - J_2 - J_1^\perp Heisenberg model on an AA-stacked bilayer honeycomb lattice

P H Y Li^{1,2} and R F Bishop^{1,2}

¹ *School of Physics and Astronomy, Schuster Building, The University of Manchester, Manchester, M13 9PL, UK*

² *School of Physics and Astronomy, University of Minnesota, 116 Church Street SE, Minneapolis, Minnesota 55455, USA*

Abstract

The regions of stability of two collinear quasiclassical phases within the zero-temperature quantum phase diagram of the spin- $\frac{1}{2}$ J_1 - J_2 - J_1^\perp model on an AA-stacked bilayer honeycomb lattice are investigated using the coupled cluster method (CCM). The model comprises two monolayers in each of which the spins, residing on honeycomb-lattice sites, interact via both nearest-neighbor (NN) and frustrating next-nearest-neighbor isotropic antiferromagnetic (AFM) Heisenberg exchange interactions, with respective strengths $J_1 > 0$ and $J_2 \equiv \kappa J_1 > 0$. The two layers are coupled via a comparable Heisenberg exchange interaction between NN interlayer pairs, with a strength $J_1^\perp \equiv \delta J_1$. The complete phase boundaries of two quasiclassical collinear AFM phases, namely the Néel and Néel-II phases on each monolayer, with the two layers coupled so that NN spins between them are antiparallel, are calculated in the $\kappa\delta$ half-plane with $\kappa > 0$. Whereas on each monolayer in the Néel state all NN pairs of spins are antiparallel, in the Néel-II state NN pairs of spins on zigzag chains along one of the three equivalent honeycomb-lattice directions are antiparallel, while NN interchain spins are parallel. We calculate directly in the thermodynamic (infinite-lattice) limit both the magnetic order parameter M and the excitation energy Δ from the $s_T^z = 0$ ground state to the lowest-lying $|s_T^z| = 1$ excited state (where s_T^z is the total z component of spin

Email address: peggyhyli@gmail.com; raymond.bishop@manchester.ac.uk (P H Y Li^{1,2} and R F Bishop^{1,2})

for the system as a whole, and where the collinear ordering lies along the z direction), for both quasiclassical states used (separately) as the CCM model state, on top of which the multispin quantum correlations are then calculated to high orders ($n \leq 10$) in a systematic series of approximations involving n -spin clusters. The sole approximation made is then to extrapolate the sequences of n th-order results for M and Δ to the exact limit, $n \rightarrow \infty$.

Keywords: honeycomb bilayer lattice, coupled cluster method, antiferromagnetism, regions of stability, collinear phases

1. Introduction

Of all the bipartite lattices in two dimensions, and in which all of the sites and all of the edges are equivalent to one another, the honeycomb lattice has the lowest value of the coordination number. Hence, it is expected to show the greatest effect of quantum fluctuations when populated by spins interacting via antiferromagnetic (AFM), isotropic Heisenberg interactions between nearest-neighbor (NN) pairs only. We also expect the largest deviations from classical behavior to occur when the spin quantum number s takes the lowest value, $s = \frac{1}{2}$. It is only natural therefore for spin- $\frac{1}{2}$ models on the (infinite) two-dimensional (2D) honeycomb lattice to play a special role in the study of quantum phase transitions (QPTs), since lower values of the system dimensionality d also tend to favor the enhancement of quantum effects. One of the most directly observable such effects of quantum fluctuations will be to reduce the value of the order parameter M (defined to be the average local onsite magnetization or, equivalently, the sublattice magnetization for bipartite lattices) from its classical value equal to s , either to zero or to some nonzero value.

For the simplest, unfrustrated Heisenberg antiferromagnet (HAF) with NN exchange interactions only, all of equal strength $J_1 > 0$, on a 2D monolayer honeycomb lattice, it is by now well established that the perfect Néel long-range order (LRO) that exists in the classical ($s \rightarrow \infty$) limit, i.e., $M = s$, is not destroyed totally by quantum fluctuations for any finite value of s . Rather, M is reduced from its classical value, but to a value still greater than zero. For example, for the extreme quantum case $s = \frac{1}{2}$, the Néel order parameter is reduced by nearly half from its classical value, taking the value $M \approx 0.27$ [1, 2]. Accordingly, it is now interesting to enquire about how the Néel LRO on the honeycomb monolayer might be destroyed by the

inclusion of additional competing interactions to the NN AFM bonds. Two straightforward means to do so are now considered, one involving frustration and other without.

The first method is to include isotropic AFM Heisenberg exchange bonds between next-nearest-neighbor (NNN) pairs of spins, all with equal strength, $J_2 \equiv \kappa J_1$. If $J_2 > 0$, the J_2 bonds clearly act to frustrate the Néel order promoted by the $J_1 > 0$ bonds. The resulting J_1 - J_2 model thus obtained has been much studied on the honeycomb lattice, particularly for the case $s = \frac{1}{2}$, using a large cross-section of available analytical and numerical techniques [3–22]. The second method to include additional competing bonds, now without frustration, is to take two identical honeycomb monolayers and arrange them into an *AA*-stacked bilayer (i.e., with each site of one monolayer placed immediately above its equivalent on the other monolayer), and now add a NN interlayer Heisenberg exchange coupling so that all such bonds have equal strength, $J_1^\perp \equiv \delta J_1$. Such interlayer J_1^\perp bonds do not directly frustrate the Néel LRO promoted by the intralayer J_1 bonds. Indeed, at the classical level ($s \rightarrow \infty$) they have no effect at all. Nevertheless, for finite values of s , the J_1 and J_1^\perp bonds are in competition with one another since the J_1^\perp bonds acting alone will promote the formation of interlayer NN dimers (i.e., spin-singlet pairs in the case $J_1^\perp > 0$, and spin-triplet pairs when $J_1^\perp < 0$). Thus, the inclusion of the J_1^\perp bonds leads to a competition between a phase with Néel magnetic LRO on each monolayer and a nonclassical paramagnetic phase of the valence-bond crystalline (VBC) kind and formed of interlayer dimers. The resulting J_1 - J_1^\perp model, and its Néel to dimer quantum phase transition, has been studied on the bilayer honeycomb lattice, for the cases of spins with $s = \frac{1}{2}, 1, \frac{3}{2}$, using both exact stochastic series expansion quantum Monte Carlo (QMC) simulation algorithms and an approximate analysis based on a bond operator method that has been generalized to arbitrary values of s [23].

More recently there have been some initial studies of the so-called J_1 - J_2 - J_1^\perp model on the bilayer honeycomb lattice, in which both types of competition discussed above to destroy Néel order act simultaneously [24–27]. In the earlier work [24, 25] the model was studied using Schwinger-boson mean field theory, augmented by the exact diagonalization of a relatively small (24-site) cluster, linear spin-wave theory, and a calculation of the spin-triplet energy gap using a dimer series expansion carried out to relatively low (viz., fourth) orders. In our own later work [26, 27] we studied the model for the case $s = \frac{1}{2}$ using a high-order implementation of a fully microscopic quantum

many-body theory technique, namely the coupled cluster method (CCM), which yielded accurate results for the ground-state (GS) energy per spin, the Néel magnetic order parameter M , the excitation energy Δ from the $s_T^z = 0$ ground state to the lowest-lying $|s_T^z| = 1$ excited state (where s_T^z is the total z component of spin for the system as a whole, and where the collinear ordering lies along the z direction), and the zero-field transverse (uniform) magnetic susceptibility χ in the Néel phase. We thus obtained in particular an accurate estimate for the full phase boundary of the Néel phase in the quadrant with $\kappa > 0$ and $\delta > 0$ of the $\kappa\delta$ plane of the zero-temperature ($T = 0$) quantum phase diagram.

We note that the CCM [28–43] has itself been applied with great success to a very wide array of systems in quantum magnetism, in almost all of which it has yielded results which are either the most accurate or among the most accurate available. In particular, these encompass a considerable number of applications to a variety of frustrated monolayer honeycomb-lattice models [15–17, 44–53], including the spin- $\frac{1}{2}$ J_1 – J_2 model itself [16, 17]. Apart from the Néel AFM state exhibited by this model at low values of the frustration parameter $\kappa \equiv J_2/J_1$, several accurate calculations (and see, e.g., Refs. [5, 11, 14, 22]), including those using the CCM [15–17], show that it also exhibits another quasiclassical phase with collinear magnetic LRO, viz., the so-called Néel-II phase described in more detail in Sec. 2, for higher values of κ . In between these two quasiclassical magnetic phases there is also broad agreement between calculations based on a variety of different techniques that the system is paramagnetic, with VBC order of the plaquette (PVBC) and/or staggered dimer (SDVBC or, equivalently, lattice nematic) type. There have also been hints of possible small regions of κ beyond the Néel regime where the stable GS phase may be a quantum spin liquid (QSL).

In view of the richness and complexity of the spin- $\frac{1}{2}$ J_1 – J_2 model on a monolayer honeycomb lattice, it is clearly of great interest to investigate the comparable spin- $\frac{1}{2}$ J_1 – J_2 – J_1^\perp model on the honeycomb bilayer. Of particular interest will be to investigate the stability and sensitivity of the various GS phases exhibited by the monolayer to the degree of interlayer coupling, $\delta \equiv J_1^\perp/J_1$, that is present. To date the only calculations performed on this model (in *AA* stacking), to our knowledge, have been to investigate the stability of the Néel phase in the $\kappa\delta$ plane for $\kappa > 0$ and $\delta > 0$ [24–27]. In the present paper our aim is to extend those earlier preliminary calculations to include both quasiclassical AFM GS phases (viz., the Néel and Néel-II phases) present when $\delta = 0$, and to investigate their realms of stability

in the entire $\kappa\delta$ half-plane with intralayer frustration (i.e., $\kappa > 0$). In so doing we will shed considerable light on the extraordinary sensitivity of *both* phases on the honeycomb monolayer, specifically by showing explicitly how their corresponding phase boundaries change rapidly as functions of κ in the region of small interlayer coupling δ .

The plan of the rest of the paper is as follows. We first describe the J_1 – J_2 – J_1^\perp model itself in Sec. 2, including a description of its main features in the limiting case, $J_1^\perp \rightarrow 0$, of the monolayer. In Sec. 3 we briefly review the main features of the CCM, before presenting our results for the Néel and Néel-II phases obtained from using it in Sec. 4. The results are then discussed and summarized in Sec. 5.

2. The model

The J_1 – J_2 – J_1^\perp model on the bilayer honeycomb lattice is specified by the Hamiltonian

$$\begin{aligned} H &= J_1 \sum_{\langle i,j \rangle, \alpha} \mathbf{s}_{i,\alpha} \cdot \mathbf{s}_{j,\alpha} + J_2 \sum_{\langle\langle i,k \rangle\rangle, \alpha} \mathbf{s}_{i,\alpha} \cdot \mathbf{s}_{k,\alpha} \\ &\quad + J_1^\perp \sum_i \mathbf{s}_{i,A} \cdot \mathbf{s}_{i,B} \\ &\equiv J_1 h(\kappa, \delta); \quad \kappa \equiv J_2/J_1, \quad \delta \equiv J_1^\perp/J_1, \end{aligned} \tag{1}$$

where the index i labels the sites on each (horizontal) monolayer (i.e., in AA stacking, so that corresponding sites i on the top layer lie vertically above those on the lower layer), and the index $\alpha = A, B$ labels the two layers. Each site (i, α) carries a spin- s particle described by the usual $SU(2)$ spin operators $\mathbf{s}_{i,\alpha} \equiv (s_{i,\alpha}^x, s_{i,\alpha}^y, s_{i,\alpha}^z)$, with $\mathbf{s}_{i,\alpha}^2 = s(s+1)\mathbb{1}$. We restrict ourselves here to the extreme quantum case, $s = \frac{1}{2}$. The first two sums in Eq. (1) over $\langle i, j \rangle$ and $\langle\langle i, k \rangle\rangle$ run respectively over all NN and NNN intralayer pairs of spins on each monolayer honeycomb lattice, counting each Heisenberg bond (with strengths J_1 and J_2 respectively) once and once only. The third sum in Eq. (1) describes the interlayer Heisenberg bonds, with strength J_1^\perp , between NN pairs of spins across the two AA -stacked monolayers (i.e., at the same horizontal site index i).

We are interested here in the case when both intralayer bonds are AFM in nature (i.e., $J_1 > 0$, $J_2 > 0$). Since the parameter J_1 simply sets the overall energy scale, we may write the Hamiltonian as in the last line in Eq.

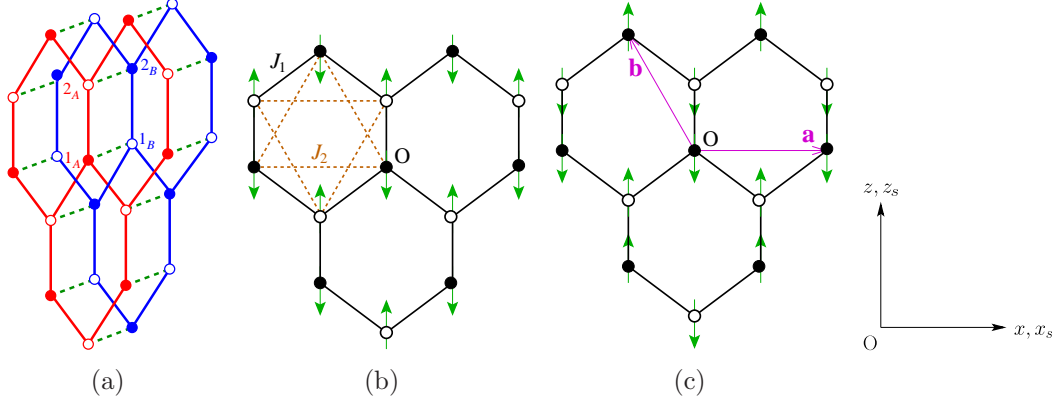


Figure 1: The J_1 - J_2 - J_1^\perp model on the bilayer honeycomb lattice, showing (a) the two layers A (red) and B (blue), the nearest-neighbor (NN) bonds ($J_1 = \text{---}$; $J_1^\perp = \text{- - -}$) and the four sites ($1_A, 2_A, 1_B, 2_B$) of the unit cell; (b) the intralayer bonds ($J_1 = \text{---}$; $J_2 = \text{- - -}$) on each monolayer and the monolayer Néel state; and (c) the triangular Bravais lattice vectors \mathbf{a} and \mathbf{b} , and one of the three equivalent monolayer Néel-II states. Sites ($1_A, 2_B$) and ($2_A, 1_B$) on the two triangular lattices of each monolayer are shown by filled and empty circles respectively, and the spins are represented by the (green) arrows on the lattice sites. For both states on the bilayer, spins on NN sites between the two layers are antiparallel.

(1), where the relevant parameters are thus $\kappa \equiv J_2/J_1$ and $\delta \equiv J_1^\perp/J_1$. The lattice and the Heisenberg exchange bonds are illustrated in Figs. 1(a) and 1(b). We thus restrict attention here to investigating the stability of the two quasiclassical collinear AFM phases in the $\kappa\delta$ half-plane with $\kappa > 0$. The spin patterns of these two phases on each monolayer, viz., the Néel and Néel-II states, are shown respectively in Figs. 1(b) and 1(c). Whereas the Néel state has all three NN spins to a given spin antiparallel to it, the Néel-II state has two such spins antiparallel and one parallel. The Néel state may equivalently be described as having AFM sawtooth (or zigzag) chains along all three of the equivalent honeycomb-lattice directions. By contrast, each Néel-II state has AFM sawtooth along only one of the honeycomb directions [e.g., along the \hat{x} direction in Fig. 1(c)], and now with NN spins on adjacent chains parallel to each other. There are thus two other equivalent Néel-II states to that shown in Fig. 1(c), obtained from it by rotations in the xz plane by $\pm 120^\circ$ about the center of any hexagon. The Néel-II states thus break the lattice rotational symmetry that is preserved by the Néel state by contrast. Whereas the Néel state has a 2-site unit cell structure, the Néel-II state has

a 4-site structure. Since the Néel-II state also comprises collinear stripes of parallel spins [i.e., along lines parallel to the z -axis in Fig. 1(c)] that alternate in direction, it is also sometimes called the collinear striped AFM phase in the literature. We note that we prefer to avoid this terminology, since it is open to considerable confusion with other AFM states on the honeycomb lattice that are also known as striped states (and see, e.g., Ref. [15]) and which comprise sawtooth chains of parallel spins that alternate in direction.

While the honeycomb lattice is bipartite, it is non-Bravais. It comprises two interpenetrating triangular Bravais sublattices 1 and 2, with lattice vectors $\mathbf{a} = \sqrt{3}d\hat{x}$ and $\mathbf{b} = \frac{1}{2}d(-\sqrt{3}\hat{x} + 3\hat{z})$, as shown in Fig. 1(c), where each monolayer is defined to lie in an xz plane, as illustrated in Fig. 1, and d is the honeycomb lattice spacing (i.e., the separation distance between NN pairs on the hexagonal lattice). Each monolayer unit cell l at position vector $\mathbf{R}_l = m_l\mathbf{a} + n_l\mathbf{b}$, where $m_l, n_l \in \mathbb{Z}$, thus comprises the two sites at \mathbf{R}_l on sublattice 1 and $\mathbf{R}_l + d\hat{z}$ on sublattice 2. The corresponding four sites of the AA-stacked bilayer honeycomb lattice unit cell are shown in Fig. 1(a).

Clearly, the reciprocal lattice vectors that correspond to the real-space vectors \mathbf{a} and \mathbf{b} may be taken as $\boldsymbol{\alpha} = 2\pi(\sqrt{3}\hat{x} + \hat{z})/(3d)$ and $\boldsymbol{\beta} = 4\pi/(3d)\hat{z}$. The parallelograms formed by the pairs of vectors (\mathbf{a}, \mathbf{b}) and $(\boldsymbol{\alpha}, \boldsymbol{\beta})$ are thus the Wigner-Seitz unit cell and the first Brillouin zone, respectively, of the monolayer honeycomb lattice. Equivalently, both may be taken to be centered on a point of sixfold rotational symmetry in their corresponding spaces. In this case the Wigner-Seitz unit cell is bounded by the sides of a primitive hexagon of side length d , as in Fig. 1, and the corresponding first Brillouin zone is then also a hexagon, now of side length $4\pi/(3\sqrt{3}d)$, but rotated by 90° with respect to the Wigner-Seitz hexagon. Thus, with respect to an origin at the center of the hexagon, three of its corners occupy the positions $\mathbf{K}^{(1)} = 4\pi/(3\sqrt{3}d)\hat{x}$, $\mathbf{K}^{(2)} = 2\pi(\hat{x} + \sqrt{3}\hat{z})/(3\sqrt{3}d)$, and $\mathbf{K}^{(3)} = 2\pi(-\hat{x} + \sqrt{3}\hat{z})/(3\sqrt{3}d)$, with the remaining corners at positions $\mathbf{K}^{(n+3)} = -\mathbf{K}^{(n)}$; $n = 1, 2, 3$.

Classically, the generic stable GS phase with magnetic LRO takes the form of a coplanar spiral configuration of spins defined in terms of an ordering wave vector \mathbf{Q} , plus an angle θ that measures the angle between the two spins in each monolayer unit cell l at position vector \mathbf{R}_l . The two classical spins, each of length $s(\rightarrow \infty)$, in unit cell l , are written as

$$\mathbf{s}_{l,\rho} = -s[\cos(\mathbf{Q} \cdot \mathbf{R}_l + \theta_\rho)\hat{z}_s + \sin(\mathbf{Q} \cdot \mathbf{R}_l + \theta_\rho)\hat{x}_s]; \quad \rho = 1, 2, \quad (2)$$

where the index ρ labels the two sites in the unit cell, and \hat{x}_s and \hat{z}_s are

two orthogonal unit vectors that define the spin-space plane, as illustrated in Fig. 1. With no loss of generality, we may choose the two angles θ_ρ such that $\theta_1 = 0$ and $\theta_2 = \theta$ for the spins on triangular sublattices 1 and 2, respectively.

Within this framework the Néel GS spin configuration shown in Fig. 1(b) is now specified by the ordering wave vector $\mathbf{Q} = \mathbf{\Gamma} = (0, 0)$, together with the value $\theta = \pi$ for the relative angle variable between the two sites in the unit cell. Similarly, the Néel-II GS spin configuration shown in Fig. 1(c) is specified by the ordering wave vector $\mathbf{Q} = \mathbf{M}^{(2)} = 2\pi/(3d)\hat{z}$, together with the value $\theta = 0$. We note that $\mathbf{M}^{(2)}$ is just the vector that defines the midpoint of the edge joining the corners $\mathbf{K}^{(2)}$ and $\mathbf{K}^{(3)}$ of the hexagonal first Brillouin zone described above. Thus, the other two inequivalent Néel-II states have ordering wave vectors that correspond to the midpoints of the other two non-parallel edges of the hexagonal first Brillouin zone, and in each case now together with the value $\theta = \pi$ for the relative angle variable between the two sites on the monolayer unit cell shown in Fig. 1(a). These may hence be taken as $\mathbf{Q} = \mathbf{M}^{(1)} = \pi(\sqrt{3}\hat{x} + \hat{z})/(3d)$ and $\mathbf{Q} = \mathbf{M}^{(3)} = \pi(-\sqrt{3}\hat{x} + \hat{z})/(3d)$, which are, respectively, the midpoints of the edges joining corners $\mathbf{K}^{(1)}$ and $\mathbf{K}^{(2)}$, and corners $\mathbf{K}^{(3)}$ and $\mathbf{K}^{(4)}$.

Note that, equivalently, we have $\mathbf{M}^{(1)} = \frac{1}{2}\boldsymbol{\alpha}$, $\mathbf{M}^{(2)} = \frac{1}{2}\boldsymbol{\beta}$, $\mathbf{M}^{(3)} = \frac{1}{2}(\boldsymbol{\beta} - \boldsymbol{\alpha})$. Hence, each of the Néel-II states corresponds to an ordering wave vector that equals exactly one half of a reciprocal lattice vector. While the generic stable classical GS phase is described by the spin configuration of Eq. (2), it is also known [54] that exceptions occur if the ordering wave vector \mathbf{Q} takes a value equal to one half or one quarter of a reciprocal lattice vector $\mathbf{G}_i \equiv k_i\boldsymbol{\alpha} + l_i\boldsymbol{\beta}$, with $k_i, l_i \in \mathbb{Z}$, as for the Néel-II states. In this case the classical GS phase is a two-dimensional manifold that continuously connects the three $\mathbf{Q} = \mathbf{M}^{(i)}$ states with $i = 1, 2, 3$, which now leads to an infinitely degenerate family (IDF) of non-planar ground states [5]. As expected, it can then be shown (and see Ref. [5] for details) that the effect of quantum fluctuations in leading order (i.e., in the large- s limit using linear spin-wave theory) is to stabilize the collinear Néel-II phases from among the IDF family of solutions.

For the classical ($s \rightarrow \infty$) J_1 - J_2 model on the monolayer honeycomb lattice, one may show that one value of the ordering wave vector \mathbf{Q} that minimizes the GS energy is given by

$$\mathbf{Q} = \frac{2}{\sqrt{3}d} \cos^{-1} \left(\frac{1 - 2\kappa}{4\kappa} \right) \hat{x}, \quad (3)$$

which should be taken together with the value $\theta = \pi$ for the relative phase

angle. Clearly, the spiral pitch angle in Eq. (3) is physical only when $\kappa \geq \frac{1}{6}$, and at the boundary $\kappa = \frac{1}{6}$ we have $\mathbf{Q} = 0$. One finds that the Néel state (with $\mathbf{Q} = 0$) is the stable GS phase for all values $\kappa \leq \frac{1}{6}$, and a spiral state forms the GS phase for $\frac{1}{6} < \kappa < \infty$. We note that as $\kappa \rightarrow \infty$, which is the point where the two triangular sublattices of the honeycomb lattice decouple, the spiral pitch angle takes the value $\pm \frac{2}{3}\pi$, which is just the expected classical spin ordering for a triangular lattice. In this limit the ordering wave vector \mathbf{Q} of Eq. (3) approaches the value $\mathbf{K}^{(1)}$ of one of the corners of the hexagonal first Brillouin zone. Clearly, there are also five other symmetry-related \mathbf{Q} values for the spiral phase that minimize the classical GS energy in this case, which are obtained by rotations $\frac{1}{3}n\pi$, with $n = 1, 2, 3, 4, 5$, of the \mathbf{Q} vector of Eq. (3).

In fact, it can readily be shown [3, 5, 6] that for all values $\kappa > \frac{1}{6}$ the classical J_1 - J_2 model on the monolayer honeycomb lattice actually has an IDF of incommensurate, planar, spin spiral GS phases in which the spiral wave vector \mathbf{Q} can point in an arbitrary direction. For each value of the frustration parameter in the range $\frac{1}{6} < \kappa < \frac{1}{2}$ these classically degenerate solutions form a closed contour around the center, $\mathbf{Q} = \mathbf{\Gamma} = (0, 0)$, of the hexagonal first Brillouin zone. Conversely for each value $\kappa > \frac{1}{2}$ the solutions lie on pairs of closed contours centered on any two of the inequivalent corners (say $\mathbf{K}^{(1)}$ and $\mathbf{K}^{(2)}$) of the hexagonal first Brillouin zone. Precisely at the classical critical point $\kappa = \frac{1}{2}$, which marks the transition between two different spiral phases, the contour for the degenerate values of \mathbf{Q} is formed from the hexagon joining the midpoints $\mathbf{M}^{(n)}$ of the six edges of the hexagonal first Brillouin zone. It is easy to see that this boundary can equivalently be taken as a pair of equilateral triangles centered on $\mathbf{K}^{(1)}$ and $\mathbf{K}^{(2)}$, respectively, for the first of which one of its sides is the line joining $\mathbf{M}^{(6)}$ and $\mathbf{M}^{(1)}$, and for the second of which one of its sides is the line joining $\mathbf{M}^{(1)}$ and $\mathbf{M}^{(2)}$. At the critical point $\kappa = \frac{1}{2}$, the value of \mathbf{Q} from Eq. (3) is precisely the midpoint of the line joining the corners $\mathbf{M}^{(1)}$ and $\mathbf{M}^{(6)}$. We also note that precisely at this critical point $\kappa = \frac{1}{2}$ the spiral phases are also degenerate with the collinear Néel-II phase. As $\kappa \rightarrow \infty$, the contours collapse to the points $\mathbf{K}^{(1)}$ and $\mathbf{K}^{(2)}$ themselves.

At leading order in spin-wave theory quantum fluctuations have been shown [6] to lift this otherwise accidental degeneracy in favor of specific wave vectors that now minimize the GS energy from among each IDF of states, thereby leading to the phenomenon of spiral order by disorder [54–56]. As the frustration parameter κ is increased from the value $\frac{1}{6}$ to the value $\frac{1}{2}$, one

solution for this selected set of values for \mathbf{Q} moves continuously along the straight line from the point $\mathbf{Q} = \mathbf{\Gamma} = (0, 0)$ to the point $\mathbf{Q} = \mathbf{M}^{(2)}$. As κ is then increased further to values greater than $\frac{1}{2}$, this selected value for \mathbf{Q} then moves continuously along an edge of the hexagonal first Brillouin zone from $\mathbf{M}^{(2)}$ to the corner $\mathbf{K}^{(2)}$. For all values $\kappa > \frac{1}{6}$, there are clearly still six symmetry-related degenerate values of \mathbf{Q} that are so selected by quantum fluctuations, with the other five, in each case, related to those described above by rotations about $\mathbf{\Gamma} = (0, 0)$ of $\frac{1}{3}n\pi$, with $n = 1, 2, 3, 4, 5$.

For the extreme quantum case $s = \frac{1}{2}$, one expects that quantum fluctuations might well be sufficiently strong as to melt the coplanar spiral order, in favor of either collinear quasiclassical magnetic orderings or nonclassical paramagnetic states, over a wide range of values of κ for the J_1 - J_2 model on the monolayer honeycomb lattice. Similarly, since, in general, quantum fluctuations tend to favor collinear over non-collinear order, one expects that the critical value $\kappa_c^{1,>}$ of the frustration parameter κ beyond which Néel order melts might be larger than the classical value of $\frac{1}{6}$ for the spin- $\frac{1}{2}$ J_1 - J_2 model on the monolayer honeycomb lattice. By now there is a broad consensus among authors using a wide variety of calculational techniques (see, e.g., Refs. [10–22]) that both of these conjectures are true. In particular, the majority of calculations yield a value for $\kappa_c^{1,>}$ in the approximate range 0.19 to 0.23. There is then some controversy about whether the Néel state is followed immediately by a paramagnetic PVBC state or whether there is a small intermediate QSL phase. Beyond the region of stability of the PVBC phase many calculations concur that the classical spin spiral states are still destabilized for a further range of values of κ in favor of a stable GS phase that is either a paramagnetic SDVBC state or a quasiclassical Néel-II AFM state (or, indeed, different regimes of both). Since both the SDVBC and Néel-II states break the same lattice symmetries, many calculations find them very difficult to differentiate cleanly. This is particularly true for methods (such as exact diagonalization and density-matrix renormalization group techniques) that are based intrinsically on finite-size lattices, and which need to be extrapolated to the infinite-lattice ($N \rightarrow \infty$) limit.

One of our aims in the present paper is to shed more light on the stability of both possible quasiclassical AFM phases of the spin- $\frac{1}{2}$ J_1 - J_2 model on the monolayer honeycomb lattice, viz., the Néel and Néel-II phases. In order to do so we now consider the larger spin- $\frac{1}{2}$ J_1 - J_2 - J_1^\perp model on the bilayer honeycomb lattice, and consider the realms of stability of both phases in the $\kappa\delta$ half-plane with $\kappa \equiv J_2/J_1 > 0$ (and $J_1 > 0$), and for arbitrary values

of the interlayer coupling parameter, $\delta \equiv J_1^\perp/J_1$. While we consider both signs of δ , we will principally be interested in the case of an AFM interlayer coupling ($J_1^\perp > 0$), such that NN spins between the two layers of the *AA*-stacked bilayer are antiparallel to one another. Thus, it is important to note from the outset that although we will also consider cases with $J_1^\perp < 0$, where physically the NN spins between the two layers would energetically prefer to be parallel to one another, we consider here only the stability of the two phases with each monolayer having either Néel or Néel-II ordering, but with the two layers connected so that NN spins between them are antiparallel. Obviously these bilayer phases are unphysical when $\delta < 0$. Nevertheless, we study them also in this unphysical regime, as well as in the physical regime where $\delta > 0$, since by doing so we can shed particular light on the stability of the two collinear monolayer phases (i.e., when $\delta = 0$). As a foretaste of our results, we remark that we will demonstrate rather clearly why both phase boundaries for the monolayer are difficult to calculate with high accuracy, by showing how sensitive the boundaries in the bilayer model are to small changes in δ near the monolayer limit, $\delta = 0$.

3. The coupled cluster method

The CCM provides an accurate and versatile technique of *ab initio* quantum many-body theory, which has been applied with considerable success in a wide range of physical and chemical contexts (and see, e.g., Refs. [31–33, 35, 38, 40, 41, 43, 57]). Very importantly, the method is systematically improvable within several well-defined hierarchical approximation schemes that are guaranteed to approach the exact results in the limit $n \rightarrow \infty$, where n is an index that signifies the order of the approximation within some specified scheme. Of course, computational considerations generally restrict one in practice to the highest values n in the sequence that are attainable, and one then needs to extrapolate the partial sequences of values obtained for any GS or excited-state (ES) parameter to the limit $n \rightarrow \infty$, as we describe below.

It is important to realize from the outset that this extrapolation to the exact physical limit ($n \rightarrow \infty$) is the *only* approximation that ever needs to be made when implementing the CCM in practice. In particular, since the method is both size-extensive and size-consistent at every approximation level n , it can be implemented from the very beginning in the infinite system ($N \rightarrow \infty$) limit. This immediately removes the need for any finite-size scaling

of the sort that is required by most alternative methods such as, for example, the exact diagonalization (ED) of small lattices and density-matrix renormalization group (DMRG) techniques. This additional associated source of errors is thus circumvented by use of the CCM.

In addition to these obvious advantages the CCM has two other important attributes. Thus, at every n th-order level of approximation, the CCM also exactly preserves both the Hellmann-Feynman theorem and the Goldstone linked cluster theorem. These attributes are key to understanding the success of the method in providing results for a variety of both GS and ES parameters for the system being studied that are both highly accurate and also self-consistent. By now these include a large number of spin-lattice systems in quantum magnetism, and accordingly we refer the reader to the extensive literature (and see, e.g., Refs. [2, 15–17, 26, 27, 42–53] and references cited therein) for complete details. Nevertheless, we present below a brief recapitulation of those features of the method that are most germane to the present analysis.

In order to initiate any application of the CCM one needs first to choose some (one or more) suitable normalized model (or reference) state $|\Phi\rangle$, on top of which the quantum correlations present in the exact GS or ES wave functions appropriate to the phase of the system under study are then (in principle exactly) incorporated in terms of correlations operators that involve a very specific exponentiated form, which is one of the distinguishing key features of the method. It is then these correlations operators that are systematically approximated to higher and higher orders, as discussed above, and to which we return in more detail below. In order to calculate the stability regimes of the GS phases discussed here, we utilize (separately) both the quasiclassical AFM states (viz., the Néel and Néel-II states, as illustrated in Figs. 1(b) and 1(c), respectively) for each honeycomb-lattice monolayer, as our two choices for CCM model state. Both of the quasiclassical AFM states are eigenstates of the operator s_T^z , where $s_T^z \equiv \sum_{k,\alpha} s_{k,\alpha}^z$ is the total z component of spin for the system as a whole, using global spin axes, with $s_T^z = 0$. For each collinear phase we also present results for the excitation energy Δ from the corresponding $s_T^z = 0$ ground state to the lowest-lying excited state in the $|s_T^z| = 1$ sector.

Once the choice of model state has been made the only remaining decision before the CCM can be implemented computationally is the choice of approximation scheme to use. This simply involves which multispin-flip configurations that are to be retained in the GS and ES ket- and bra-state

correlation operators that are used to parametrize the corresponding exact GS and ES wave functions. We use here the very well-tested and much used scheme known as the localized lattice-animal-based subsystem (LSUB n) hierarchy. At the n th order in the LSUB n scheme those multispin-flip configurations to be retained in the CCM correlation operators are defined to be those that describe clusters of spins that span a range of n or fewer contiguous sites on the lattice. A set of lattice sites is defined to be contiguous in this sense if every site of the set is a NN to at least one other member of the set. Equivalently, in the terminology of graph theory, the LSUB n approximation retains all multispin-flip configurations defined on lattice animals (or polyominoes) of size n or smaller. We define a single spin-flip on site l and layer α as requiring the action of the spin-raising operator $s_{l,\alpha}^+ \equiv s_{l,\alpha}^x + i s_{l,\alpha}^y$ acting once on the model ket state, which is now described in the very convenient (and universal) local set of spin axes in which a different passive rotation has been made at every site so that every spin points downwards (i.e., along the negative z_s axis).

It is clear that as the truncation index $n \rightarrow \infty$ the LSUB n approximation becomes exact. We use the space- and point-group symmetries of both the system Hamiltonian and the particular CCM model state being employed to reduce the set of *independent* multi-spin configurations retained within a given LSUB n approximation to the minimal number $N_f = N_f(n)$. For example, for our system the operator s_T^z defined above is conserved, and we have that both quasiclassical AFM states lie in the sector with $s_T^z = 0$. Hence, only GS multispin-flip configurations are retained that are in accord with $s_T^z = 0$. Similarly, for the calculation of the excitation energy Δ to the lowest-lying state in the $s_T^z = 1$ conserved sector, we only retain ES multispin-flip configurations that satisfy $s_T^z = 1$. In both cases the LSUB n hierarchy is used to order the approximations. The precise way that the GS and ES correlation operators are defined is give in Ref. [26].

Nevertheless, this resulting number $N_f(n)$ of fundamental configurations typically increases rapidly as a function of the truncation index n , and the available computing power limits us in practice to a maximum value, n_{\max} . For example, for the present spin- $\frac{1}{2}$ model on the bilayer honeycomb lattice, even by making use of massively parallel supercomputing resources, both to derive (using a specially tailored computer algebra package [58]) and solve [42] the sets of N_f coupled CCM bra- and ket-state equations for both GS and ES parameters, we are constrained to $n_{\max} = 10$. Thus, we have $N_f(10) = 70\,118\, (197\,756)$ for the calculations of GS quantities for the present model using the

Néel (Néel-II) states on each monolayer as the CCM model state, respectively. The corresponding numbers of fundamental configurations retained at the LSUB10 level of approximation for the calculations of the excitation energy Δ from the $s_T^z = 0$ Néel (Néel-II) ground states to the lowest-lying excited state in the respective $s_T^z = 1$ sectors are $N_f(10) = 121\,103$ (352\,779), respectively.

In Sec. 4 we present LSUB n results for both the GS magnetic order parameter (i.e., the average local on-site magnetization) M and the excitation energy Δ to the lowest-lying state in the $s_T^z = 1$ sector, based on the use of both the Néel and Néel-II states on each monolayer as the CCM model state. Specifically, we define

$$M \equiv -\frac{1}{N} \langle \tilde{\Psi} | \sum_{k,\alpha} s_{k,\alpha}^z | \Psi \rangle, \quad (4)$$

in the local rotated spin coordinate frames described above in which each spin points along the negative z_s axis, where $\langle \tilde{\Psi} |$ and $| \Psi \rangle$ are the GS bra and ket many-body wave functions (normalized so that $\langle \tilde{\Psi} | \Psi \rangle = 1$), here parametrized in the usual CCM fashion (and see, e.g., Ref. [26] for details). Unlike in many other methods, such as QMC simulations, where quasiclassical order is naturally investigated and characterized through the parameter M^2 , it is both possible and natural within the CCM framework to calculate the parameter M directly and hence to use it to quantify the degree of order. This also has the additional advantage of showing rather clearly points where the phase under consideration becomes unstable, namely where M goes to zero and then becomes negative.

As we have noted previously, the sole approximation that now needs to be made is to extrapolate the LSUB n approximants $M(n)$ and $\Delta(n)$ for M and Δ , respectively, to the exact limit, $n \rightarrow \infty$. By now, a great deal of practical experience, from applications to many different spin-lattice models, has shown that the consistent use of simple extrapolation schemes for various physical parameters always leads to accurate results. Thus, for spin-lattice models with a high degree of frustration present, particularly in situations where the system is close to a QPT or where the order parameter M is either zero or very close to zero, the appropriate extrapolation scheme for M (and see, e.g., Refs. [15–17, 26, 27, 44–49, 52, 53, 59]) is given as

$$M(n) = \mu_0 + \mu_1 n^{-1/2} + \mu_2 n^{-3/2}, \quad (5)$$

from fits with LSUB n data sets to which we extract the LSUB ∞ extrapolant μ_0 for M . The appropriate scheme for the excitation energy Δ to the lowest-

lying state in the $s_T^z = 1$ sector is found (see e.g., Refs. [26, 50, 52, 59–62]) to be given as

$$\Delta(n) = d_0 + d_1 n^{-1} + d_2 n^{-2}. \quad (6)$$

Once again, by fitting with LSUB n data sets, we can extract the corresponding LSUB ∞ extrapolant d_0 for Δ .

There is one additional point that deserves to be mentioned in connection with the use of extrapolation schemes, such as those in Eqs. (5) or (6), in practice. This involves the possible presence of so-called “staggering effects” in the sequences of approximants. A well-known example occurs in perturbation theory where *exact* extrapolation schemes for various physical quantities are often known, but where the even and odd sequences of approximants from n th-order perturbation theory (i.e., those with $n = 2m$ and those with $n = 2m - 1$, respectively, where $m \in \mathbb{Z}^+$ is a positive integer) involve an additional staggering effect. In this case both sequences obey an extrapolation scheme of the same sort (i.e., with the same leading exponent), but where the coefficients (other than the leading constant term, corresponding to the exact, $n \rightarrow \infty$, limit) are not identical. Clearly, one should not then mix even and odd terms together in a single extrapolation scheme, unless the staggering is also incorporated explicitly. Such an explicit inclusion of the staggering is always difficult to achieve in a robust manner. In practice it is almost always circumvented by extrapolating only the even-order (or only the odd-order) terms. A similar odd/even [i.e., $(2m - 1)/2m$] staggering is also always present to a greater or lesser degree for all LSUB n sequences of approximants. It is for that reason that we restrict attention here in Sec. 4 only to even-order LSUB n approximations (i.e., those with $n = 2m$). In principle, we could also separately explore the odd-order LSUB n approximants. However, since the Hamiltonian of Eq. (1) contains only terms that are bilinear in the spin operators, it is much more natural in this case to restrict attention to the even-order approximations.

It has been noted previously [16, 17, 52, 63] that, while the $(2m - 1)/2m$ staggering in LSUB n sequences of approximants is common to all spin lattices, a further subtlety arises in the case of honeycomb-lattice models. For such models one observes an *additional* staggering effect, such that in the even-order series of LSUB n approximants for some observable quantities the terms with $n = (4m - 2)$ are offset (or staggered) with respect to those with $n = 4m$. As has been pointed out elsewhere [52], it is likely that this additional $(4m - 2)/4m$ staggering effect arises from the non-Bravais nature of

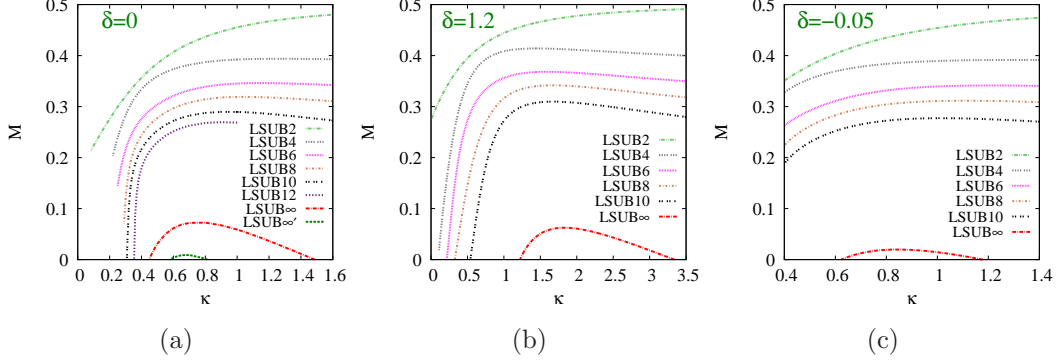


Figure 2: CCM results for the GS magnetic order parameter M versus the intralayer frustration parameter, $\kappa \equiv J_2/J_1$, for the spin- $\frac{1}{2}$ J_1 - J_2 - J_1^\perp model on the bilayer honeycomb lattice (with $J_1 > 0$), for three selected values of the scaled interlayer exchange coupling constant, $\delta \equiv J_1^\perp/J_1$: (a) $\delta = 0$, (b) $\delta = 1.2$, and (c) $\delta = -0.05$. Results based on the Néel-II state on each monolayer (and the two layers coupled so that NN spins between them are antiparallel to one another, even in case (c) where $\delta < 0$) as CCM model state are shown in LSUB n approximations with $n = 2, 4, 6, 8$, and 10 , (and also with $n = 12$ for the special case $\delta = 0$ of the J_1 - J_2 monolayer), together with the LSUB ∞ extrapolated results based on Eq. (5) and the LSUB n data sets $n = \{2, 6, 10\}$. For the case $\delta = 0$ only we also show the corresponding LSUB ∞' extrapolation based on the LSUB n data set $n = \{4, 8, 12\}$.

the honeycomb lattice. Thus, each of the two interlocking triangular Bravais sublattices, which comprise the honeycomb lattice, exhibits a $(2m - 1)/2m$ staggering of the usual kind. In turn, this then leads to the “doubling” of the effect in the composite honeycomb lattice, where it manifests itself as the observed $(4m - 2)/4m$ staggering. In order to take this additional effect into account, and since we are restricted computationally to performing LSUB n calculations for the present model to those with $n \leq 10$, most of the extrapolations discussed in Sec. 4 are based on the LSUB n data sets with $n = \{2, 6, 10\}$.

4. Results

Since the stability of the Néel phase has been discussed by us previously [26] in the sector where $\kappa > 0$ and $\delta > 0$, we concentrate attention initially on the Néel-II phase. In Fig. 2 we first show results for the magnetic order parameter M as a function of the intralayer frustration parameter $\kappa \equiv J_2/J_1$

for three separate fixed values of the interlayer coupling parameter, $\delta = 0, 1.2, -0.05$. In each case the CCM model state comprises the Néel-II state on each monolayer and the two layers connected so that NN spins between the layers are antiparallel to one another (even in the case with $\delta < 0$, where such interlayer AFM coupling is unphysical in the sense that the corresponding state with NN interlayer spins parallel to one another is clearly energetically favored). Results are shown in each case at LSUB n levels of approximation with $n = 2, 4, 6, 8$, and 10. For the special case $\delta = 0$ alone, shown in Fig. 2(a), which corresponds to the J_1 - J_2 model on the honeycomb-lattice monolayer, we also show LSUB12 results, since these are computationally feasible in this case (but not, as we have indicated previously, for the coupled bilayer cases with $\delta \neq 0$). Each of the cases shown in Fig. 2 clearly illustrates the $(4m-2)/4m$ staggering effect of the LSUB n sequences of approximations that we discussed in Sec. 3. For that reason we restrict ourselves to showing LSUB ∞ extrapolations of our LSUB n results in the general case, when $\delta \neq 0$, which are based on Eq. (5) and which use the LSUB n data sets with $n = \{2, 6, 10\}$ as input.

The results shown in Fig. 2 demonstrate very clearly that for each of the values of δ displayed there exist lower and upper critical points $\kappa_c^{2,<}(\delta)$ and $\kappa_c^{2,>}(\delta)$, such that Néel-II order exists on each of the coupled monolayers, for a given value of δ , only for values of κ in the range $\kappa_c^{2,<}(\delta) < \kappa < \kappa_c^{2,>}(\delta)$. For example, for the J_1 - J_2 monolayer ($\delta = 0$) shown in Fig. 2(a), we have $\kappa_c^{2,<}(0) \approx 0.45$ and $\kappa_c^{2,>}(0) \approx 1.49$ from the LSUB ∞ extrapolation using the LSUB n data set $n = \{2, 6, 10\}$. The corresponding values from the LSUB ∞' extrapolation using LSUB n data with $n = \{4, 8, 12\}$ are $\kappa_c^{2,<}(0) \approx 0.58$ and $\kappa_c^{2,>}(0) \approx 0.81$. While the differences between the two extrapolations may appear somewhat large, we emphasize now that these are *not* indicative of our overall errors. Rather, they arise from a specific (and wholly natural and completely unavoidable) region of great sensitivity near to the line $\delta = 0$ in the $\kappa\delta$ plane, as we explain more fully below.

It is already apparent from Fig. 2(a) that the Néel-II order in the honeycomb-lattice J_1 - J_2 monolayer is quite fragile, with values of the order parameter $M < 0.1$ over the whole range of values for κ for the values of δ shown. However, we find that as δ is first increased from zero, the interlayer coupling acts to stabilize the Néel-II phase rather rapidly, so that by the time $\delta = 0.3$ the maximum value of the order parameter is about 0.2 (at a value of κ around 0.7). In this region the values of $\kappa_c^{2,<}(\delta)$ are slightly less than $\kappa_c^{2,<}(0)$, thus exhibiting a reentrant behavior, while the values of $\kappa_c^{2,>}(\delta)$ grow mono-

tonically with δ and are appreciably greater than $\kappa_c^{2,>}(0)$. As δ is increased further, however, the interlayer coupling now acts to reduce the Néel-II order, although at the same time the range of the values of the frustration parameter κ over which it exists tends to *increase* at first. Thus, while $\kappa_c^{2,<}(\delta)$ and $\kappa_c^{2,>}(\delta)$ now both increase, the latter increases at a faster rate than the former, at least initially. We find that there exist values $\delta = \delta_2^l$ (≈ 0.2), and $\delta = \delta_2^u$ (≈ 1.2) at which, respectively, $\kappa_c^{2,<}(\delta_2^l) = \kappa_2^{\min} \approx 0.35$, and $\kappa_c^{2,>}(\delta_2^u) = \kappa_2^{\max} \approx 3.34$, such that for all values of δ we have $\kappa_c^{2,<}(\delta) \geq \kappa_2^{\min}$ and $\kappa_c^{2,>}(\delta) \leq \kappa_2^{\max}$. Figure 2(b) displays the results for M at a value $\delta = 1.2 \approx \delta_2^u$, from which we see that $\kappa_2^{\max} \approx 3.34$. As δ is now increased beyond δ_2^u , we find that $\kappa_c^{2,<}(\delta)$ continues to increase while $\kappa_c^{2,>}(\delta)$ now decreases. Finally, when δ attains the value δ_2^{\max} , the two critical values merge, $\kappa_c^{2,<}(\delta_2^{\max}) = \kappa_c^{2,>}(\delta_2^{\max}) \equiv \kappa_2^u$, such that for all values $\delta > \delta_2^{\max}$ Néel-II order is absent, whatever the value of the frustration parameter κ .

Figure 2(c) displays the effect of introducing a weak ferromagnetic interlayer coupling ($\delta < 0$) between the two monolayers with Néel-II ordering. Clearly, the already rather fragile LRO in each monolayer is now weakened further. The two critical values $\kappa_c^{2,<}(\delta)$ and $\kappa_c^{2,>}(\delta)$ move closer together as δ is made more negative, until δ reaches a value $\delta = \delta_2^{\min}$, at which value we have $\kappa_c^{2,<}(\delta_2^{\min}) = \kappa_c^{2,>}(\delta_2^{\min}) \equiv \kappa_2^l$. Néel-II order is then absent for all values $\delta < \delta_2^{\min}$, for any value of the frustration parameter κ . Based on the LSUB ∞ extrapolations, which use Eq. (5) together with the LSUB n data sets with $n = \{2, 6, 10\}$ as input, we find the values $\delta_2^{\min} \approx -0.06$ and $\kappa_2^l \approx 0.9$, together with the corresponding values at the upper boundary of Néel-II order, $\delta_2^{\max} \approx 1.51$ and $\kappa_2^u \approx 2.7$.

In Fig. 3 we exhibit the effect of the interlayer coupling on the Néel-II order in a different way by showing M versus δ curves for three separate values of the intralayer frustration parameter, $\kappa \equiv J_2/J_1$. As can be clearly seen from each of Figs. 3(a), 3(b), and 3(c), the initial effect of the interlayer AFM NN coupling, as δ is increased from zero, is to increase the order parameter M , thereby enhancing the stability of the Néel-II ordering on each monolayer. In each case the effect reaches a maximum at a certain value of δ , which depends on the specific value chosen for κ . Increasing δ further then reduce the Néel-II order, until (in the extrapolated LSUB ∞ limit) an upper critical value $\delta_2^{c,>}(\kappa)$ is reached, beyond which (for a given value of κ) Néel-II order disappears. Similarly, in each case there is a lower critical value $\delta_2^{c,<}(\kappa)$, below which Néel-II is wholly absent.

The same sort of LSUB ∞ extrapolated data that is shown in Fig. 3 is

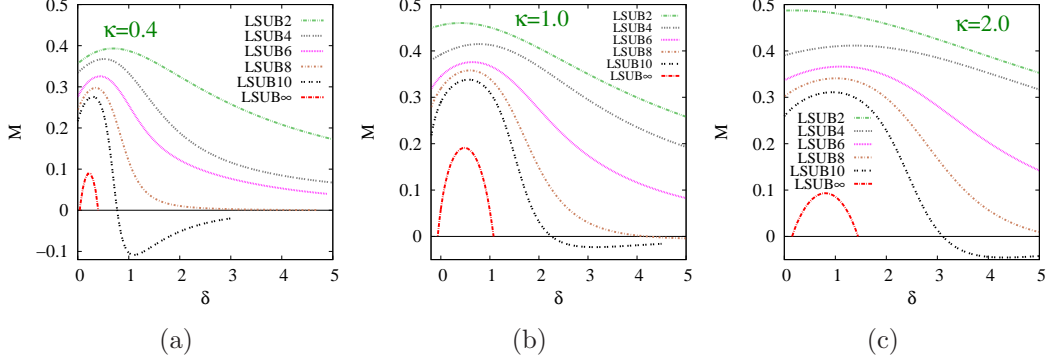


Figure 3: CCM results for the GS magnetic order parameter M versus the scaled interlayer exchange coupling constant, $\delta \equiv J_1^\perp/J_1$, for the spin- $\frac{1}{2}$ J_1 - J_2 - J_1^\perp model on the bilayer honeycomb lattice (with $J_1 > 0$), for three selected values of the intralayer frustration parameter, $\kappa \equiv J_2/J_1$: (a) $\kappa = 0.4$, (b) $\kappa = 1.0$, and (c) $\kappa = 2.0$. Results based on the Néel-II state on each monolayer (and the two layers coupled so that NN spins between them are antiparallel to one another) as CCM model state are shown in LSUB n approximations with $n = 2, 4, 6, 8$, and 10 , together with the corresponding LSUB ∞ extrapolated result based on Eq. (5) and the LSUB n data sets $n = \{2, 6, 10\}$.

also displayed in the composite Fig. 4 where we show M versus δ curves for a variety of values of the intralayer frustration parameter κ . We see very clearly that Néel-II order can exist only for values of κ in the range $\kappa_2^{\min} < \kappa < \kappa_2^{\max}$. The corresponding values of δ at which the Néel-II LRO disappears last are also observed to be $\delta_2^l \approx 0.2$ and $\delta_2^u \approx 1.2$, in accord with what was discussed previously. Similarly, the respective values of κ are also seen to be $\kappa_2^{\min} \approx 0.35$ and $\kappa^{\max} \approx 3.34$, again as already discussed above.

We consider next our CCM results for the excitation energy Δ to the lowest-lying state in the $s_T^z = 1$ sector. Thus, we first show, in Fig. 5, the corresponding results for Δ to those shown in Fig. 2 for the Néel-II magnetic order parameter M , for the same three fixed values of the interlayer coupling parameter δ . Our LSUB n results for the spin- $\frac{1}{2}$ honeycomb-lattice monolayer (i.e., for the case $\delta = 0$) are shown in Fig. 5(a). Once again, for this limiting case we can perform LSUB n approximations with $n \leq 12$, whereas for the cases $\delta \neq 0$ we are constrained to those with $n \leq 10$. Just as in Fig. 2(a) for M , so in Fig. 5(a) for Δ we show the two extrapolations: LSUB ∞ based on Eq. (6) and the input LSUB n data set $n = \{2, 6, 10\}$, and the corresponding LSUB ∞' extrapolation based on the LSUB n data set $n = \{4, 8, 12\}$. In

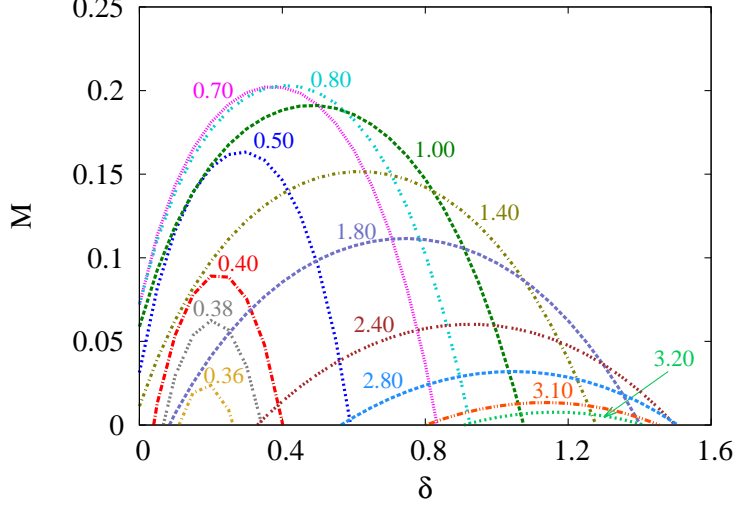


Figure 4: CCM results for the GS magnetic order parameter M versus the scaled interlayer exchange coupling constant, $\delta \equiv J_1^\perp/J_1$, for the spin- $\frac{1}{2}$ J_1 - J_2 - J_1^\perp model on the bilayer honeycomb lattice (with $J_1 > 0$), for a variety of values of the intralayer frustration parameter, $\kappa \equiv J_2/J_1$. In each case we show extrapolated results, based on the Néel-II state on each monolayer (and the two layers coupled so that NN spins between them are antiparallel to one another) as CCM model state, obtained from using Eq. (5) with the corresponding LSUB n data sets $n = \{2, 6, 10\}$.

overall terms the two extrapolations are in good agreement. In particular, both give results for Δ that are zero, up to small numerical errors, over the entire range shown with $\kappa > \kappa_2^{c,>}(0)$. This is good evidence that the QCP at $\kappa_2^{c,>}(0)$ is between two gapless states, compatible with the hypothesis that, at least for the monolayer ($\delta = 0$), the transition is from one quasiclassical state, namely the Néel-II state, to another, presumably a state with spiral order. Conversely, there is some slight evidence that at the QCP at $\kappa_2^{c,<}(0)$, the transition might be to a gapped state, presumably a VBC state.

In Figs. 5(b) and 5(c) respectively we show results for $\Delta = \Delta(\kappa)$ for the honeycomb-lattice bilayer, with the value $\delta = 1.2$ and $\delta = -0.05$ for the interlayer coupling parameter. Once again, in both cases it seems that the QCP at $\kappa_2^{c,>}(\delta)$ is from the Néel-II state to another gapless state. By contrast, our results for both of the values of δ shown in Figs. 5(b) and 5(c) indicate that the QCP at $\kappa_2^{c,<}(\delta)$ is from the quasiclassical Néel-II state to a (nonclassical) gapped state.

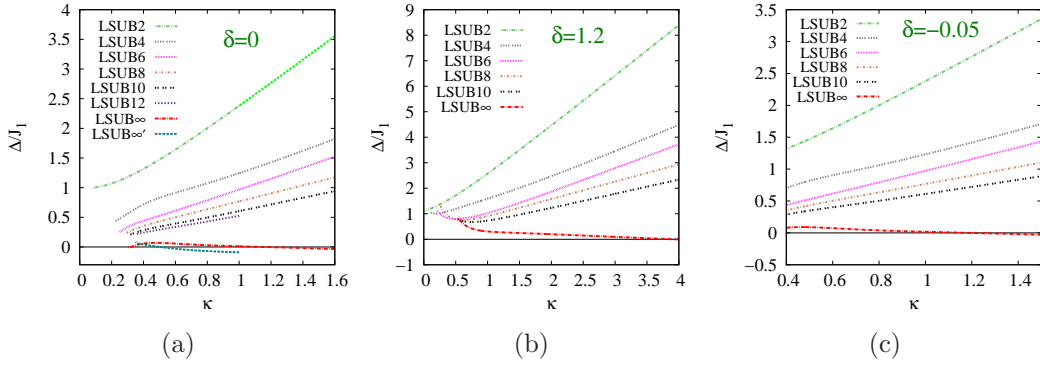


Figure 5: CCM results for the excitation energy Δ (in units of J_1) from the $s_T^z = 0$ ground state to the lowest-lying excited state with $s_T^z = 1$ versus the intralayer frustration parameter, $\kappa \equiv J_2/J_1$, for the spin- $\frac{1}{2}$ J_1 - J_2 - J_1^\perp model on the bilayer honeycomb lattice (with $J_1 > 0$), for three selected values of the scaled interlayer exchange coupling constant, $\delta \equiv J_1^\perp/J_1$: (a) $\delta = 0$, (b) $\delta = 1.2$, and (c) $\delta = -0.05$. Results based on the Néel-II state on each monolayer (and the two layers coupled so that NN spins between them are antiparallel to one another, even in case (c) where $\delta < 0$) as CCM model state are shown in LSUB n approximations with $n = 2, 4, 6, 8$, and 10, (and also with $n = 12$ for the special case $\delta = 0$ of the J_1 - J_2 monolayer), together with the LSUB ∞ extrapolated results based on Eq. (6) and the LSUB n data sets $n = \{2, 6, 10\}$. For the case $\delta = 0$ only we also show the corresponding LSUB ∞' extrapolation based on the LSUB n data set $n = \{4, 8, 12\}$.

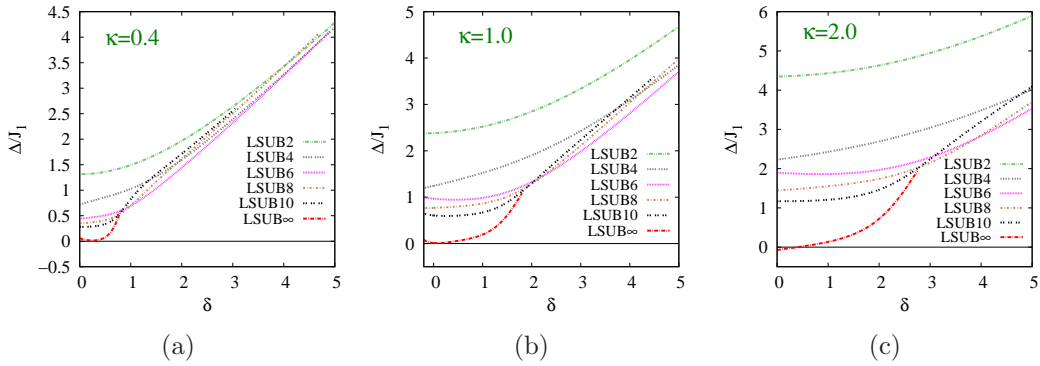


Figure 6: CCM results for the excitation energy Δ (in units of J_1) from the $s_T^z = 0$ ground state to the lowest-lying excited state with $s_T^z = 1$ versus the scaled interlayer exchange coupling constant, $\delta \equiv J_1^\perp/J_1$, for the spin- $\frac{1}{2}$ J_1 - J_2 - J_1^\perp model on the bilayer honeycomb lattice (with $J_1 > 0$), for three selected values of the intralayer frustration parameter, $\kappa \equiv J_2/J_1$: (a) $\kappa = 0.4$, (b) $\kappa = 1.0$, and (c) $\kappa = 2.0$. Results based on the Néel state on each monolayer (and the two layers coupled so that NN spins between them are antiparallel to one another) as CCM model state are shown in LSUB n approximations with $n = 2, 4, 6, 8$, and 10 , together with the corresponding LSUB ∞ extrapolated result based on Eq. (6) and the LSUB n data sets $n = \{2, 6, 10\}$. Note that, since the LSUB n curves exhibit unphysical crossings deep into the “unphysical” region where the Néel-II model state becomes less appropriate, the LSUB ∞ extrapolated curves are shown over limited ranges of values of δ .

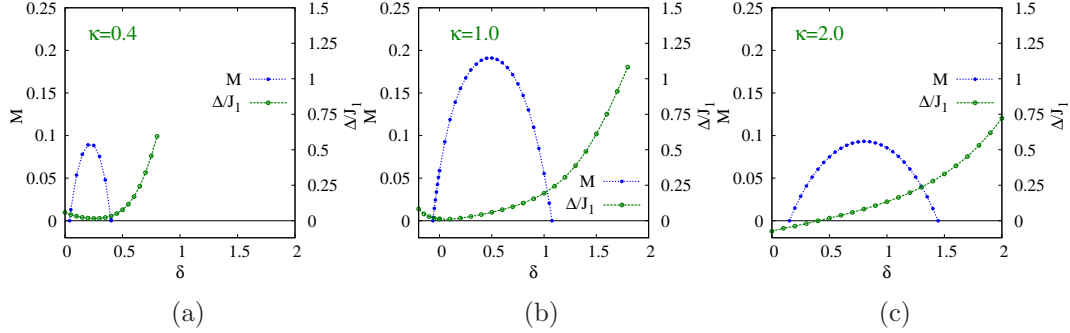


Figure 7: Juxtaposed CCM results for the magnetic order parameter M (left scale) and the excitation energy Δ (in units of J_1 , right scale) from the $s_T^z = 0$ ground state to the lowest-lying excited state with $s_T^z = 1$ versus the scaled interlayer exchange coupling constant, $\delta \equiv J_1^\perp/J_1$, for the spin- $\frac{1}{2}$ J_1 - J_2 - J_1^\perp model on the bilayer honeycomb lattice (with $J_1 > 0$), for three selected values of the intralayer frustration parameter, $\kappa \equiv J_2/J_1$: (a) $\kappa = 0.4$, (b) $\kappa = 1.0$, and (c) $\kappa = 2.0$. Extrapolated results for M and Δ are shown from using Eqs. (5) and (6), respectively, with the corresponding LSUB n data sets with $n = \{2, 6, 10\}$ in each case, based on the Néel-II state on each monolayer (and the two layers coupled so that NN spins between them are antiparallel to one another) as the CCM model state.

The effect of the interlayer coupling on the excitation energy Δ to the lowest-lying state in the $s_T^z = 1$ sector is also shown in Fig. 6 for the same three different values of the intralayer frustration parameter κ as have been shown in Fig. 3 for the Néel-II magnetic order parameter M . The LSUB ∞ extrapolations shown in each case are compatible with the phase of the system being gapless over the respective ranges of values for the interlayer coupling parameter δ for which Néel-II magnetic LRO survives according to the corresponding LSUB ∞ extrapolations for M shown in Fig. 3. We see very clearly in each case that at the upper critical point $\delta_2^{c,>}(\kappa)$ the transition is from the gapless quasiclassical Néel-II state to a (nonclassical) gapped state, which is presumably again a state with VBC order. The nature of the corresponding transitions at the lower critical points $\delta_2^{c,<}(\kappa)$ can be seen more clearly from Fig. 7, where we juxtapose our extrapolated LSUB ∞ results for $M(\delta)$ and $\Delta(\delta)$ on the same graph, for each of the three fixed values of κ shown in Figs. 3 and 6.

Of course, *all* quasiclassical states with magnetic LRO spontaneously break the continuous symmetry of the Hamiltonian of the system of Eq.

(1) under rotations in spin space. Hence, by Goldstone's theorem, the Néel-II state must have soft (Goldstone) excitation modes with a zero energy gap. The (relatively small but) nonzero values of Δ shown in Fig. 7 in the respective regions where the Néel-II magnetic order parameter M is nonzero, must hence be taken as indicative of the errors associated with extrapolating the CCM LSUB n data for the excitation energy Δ . These errors are largest in Figs. 7(a) and 7(b). However, even in these cases, a closer inspection of Fig. 6, particularly observing the LSUB10 results for both cases, clearly reveals that the deviations from zero values for the extrapolated excitation energies are very likely to be due to the (unavoidable) inclusion of the LSUB2 results in the extrapolations. Despite these numerical shortcomings, our results point to the transition at $\delta_2^{c,<}(\kappa)$ being to a gapped (and, hence, presumably a VBC) state for $\kappa = 0.4$ and 1.0 , but to a gapless (and, hence, probably a spiral quasiclassical) state for $\kappa = 2.0$.

As we have noted elsewhere (and see, e.g., Ref. [26]) for calculations performed within the CCM methodology, the vanishing of the magnetic order parameter M almost always gives a considerably more accurate estimate for the position of a QCP from a gapless to a gapped state of a system than the opening up of a nonzero value for Δ . Thus, usually at a QCP where the extrapolated value for M vanishes, the corresponding value for the slope of the curve for M as a function of the relevant coupling parameter is nonzero, precisely as is the case in Figs. 2, 3, and 4. By contrast, however, the corresponding extrapolated curves for Δ generally depart from being zero at the respective QCPs with zero slope, again precisely as we see here in Figs. 5 and 6. It is then inevitable that our CCM estimates for any such QCP from results obtained for Δ have appreciably larger associated errors than those obtained from M .

Thus, in Fig. 8 we show our final results for the $T = 0$ quantum phase diagram of the model in the $\kappa\delta$ half-plane with $\kappa > 0$, using our LSUB ∞ results for the points where the magnetic order parameter vanishes to demarcate the phase boundaries of the two collinear AFM phases, in each case with the two layers coupled so that NN spins between them are anti-aligned. Earlier results for the Néel phase [26] in the region $\delta > 0$ are also supplemented here with values $\delta < 0$, using exactly the same CCM framework as used here for the Néel-II phase, except that the Néel state on each monolayer is used as the CCM model state. Different symbols are used in Fig. 8 to distinguish between points on the phase boundaries that have been obtained from calculations at fixed values of δ (such as those in Fig. 2 for the Néel-II state) and

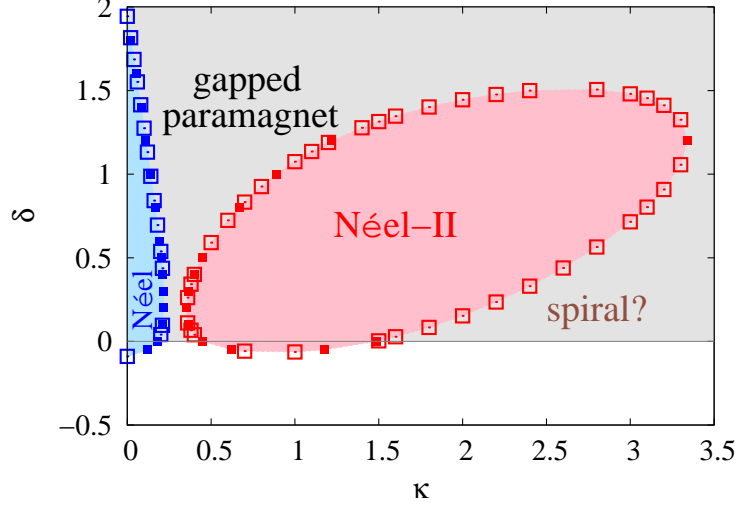


Figure 8: $T = 0$ phase diagram of the spin- $\frac{1}{2}$ J_1 - J_2 - J_1^\perp model on the bilayer honeycomb lattice with $J_1 > 0$, $\delta \equiv J_1^\perp/J_1$, and $\kappa \equiv J_2/J_1$. The blue and pink shaded regions are the quasiclassical phases with AFM Néel and Néel-II orders in each monolayer (and the two layers coupled so that NN spins across them are anti-aligned), respectively, while in the grey shaded region quasiclassical collinear order is absent. In the white unshaded region (where $\delta < 0$) there will be larger stable regions of Néel and Néel-II ordering on each monolayer but with the two layers coupled so that NN spins between them are parallel to one another, as well as phases with no collinear magnetic order. Such phases have not been investigated here. The filled and empty square symbols are points at which the extrapolated GS magnetic order parameter M for the two quasiclassical AFM phases vanishes, for specified values of δ and κ , respectively. In each case the Néel or Néel-II state on each monolayer (and the two layers coupled so that NN spins between them are antiparallel to one another, even when $\delta < 0$) is used as CCM model state, and Eq. (5) is used for the extrapolations with the corresponding LSUB n data sets $n = \{2, 6, 10\}$.

those that have been obtained from respective calculations at fixed values of κ (such as those in Fig. 3 for the Néel-II state). The fact that these two sets of critical points lie so accurately on a smooth common boundary curve for each quasiclassical collinear state is an excellent internal check on the accuracy of the extrapolation scheme of Eq. (5), which has been used to obtain them. The results are summarized and discussed in more detail in Sec. 5.

5. Discussion and Summary

The $T = 0$ quantum phase diagram of the spin- $\frac{1}{2}$ J_1 - J_2 - J_1^\perp model on an AA-stacked honeycomb bilayer lattice has been investigated here within the computational framework of the CCM. We have focussed attention on calculating the complete phase boundaries of the two collinear quasiclassical AFM phases, namely those with Néel and Néel-II magnetic LRO on each monolayer (with the two layers coupled so that NN spins between them are anti-aligned), in the half-plane $\kappa > 0$, where intralayer frustration is present, of the complete parameter space spanned by the intralayer frustration parameter, $\kappa \equiv J_2/J_1$, and the interlayer coupling strength, $\delta \equiv J_1^\perp/J_1$, for the case of AFM coupling $J_1 > 0$. The CCM has been used because it has the distinct dual advantages of satisfying both the Goldstone linked cluster theorem and the Hellmann-Feynman theorem at every level of approximation that we use. In these two important regards the method is essentially unequalled by any other technique of *ab initio* quantum many-body theory that can be applied to such spin-lattice systems as we study here. One consequence is that we have been able to perform all of our calculations in the thermodynamic (infinite lattice, $N \rightarrow \infty$) limit from the outset, thereby obviating the need for any finite-size scaling of our results. Since such scaling is usually an important source of errors in competing methods, and since finite systems often do not share the same GS ordering as their infinite counterparts, it is a real strength of our calculations that we have been able to circumvent these issues.

Nevertheless, of course, we have necessarily had to make approximations. However, we have done so within the context of a well-defined hierarchy of truncations for the CCM multispin correlations that are retained (viz., the so-called LSUB n scheme), which has been rigorously tested on many previous occasions in applications to a large number of strongly correlated and highly frustrated quantum spin-lattice models. The approximations are guaranteed to become exact in the limit that the truncation order becomes infinite ($n \rightarrow \infty$), and our sole approximation for the calculation of any physical parameter is to perform this extrapolation on the corresponding LSUB n sequences of approximants that are computationally feasible to perform. For the present model we have been able to implement the method for calculations of both the magnetic order parameter M and the excitation energies Δ from the $s_T^z = 0$ collinear ground states to the lowest-lying respective states in the conserving $s_T^z = 1$ sectors, to very high orders, namely those with $n \leq 10$.

While there exist by now very well-tested and much studied LSUB n extrapolation schemes for the quantities M and Δ among others, an additional complication arises in the case of the honeycomb lattice, which manifests itself as a $(4m - 2)/4m$ staggering effect in the sequences of LSUB n approximants, and which we have discussed in detail in Sec. 3. Since its origin almost certainly lies in the non-Bravais nature of the honeycomb lattice, it is important to realize that its effect is unavoidable and *must* be taken into account when high accuracy is required. Indeed, it is a testament to the power and accuracy of the CCM that this additional staggering has been clearly observed here. Naturally, it is possible, even likely, that the same or related staggering effects also occur in other calculational schemes, where they have perhaps been overlooked hitherto.

For reasons that we have enumerated, our most accurate calculations for the phase boundaries on which Néel or Néel-II magnetic LRO melts come from the points where the respective order parameter M vanishes. Nevertheless, our results for Δ provide excellent independent corroboration of the regions in which quasiclassical magnetic order is present (i.e., where Δ vanishes), while also giving some additional information on whether the transition from one of the collinear AFM states at a given point on a boundary is to a gapped or a gapless state.

It is perhaps worth noting at this point that we have not attempted to implement any wave vector optimization to search for a *lowest* spin gap. In the first place any such attempt would add very significantly to the computational burden of what is already a set of calculations that push at the limit of what can be performed at the very high LSUB10 level of approximation that is required for accuracy in these calculations, even with the use of powerful supercomputing resources. Indeed, any such wave vector optimization, at the required level of implementation to give accurate, meaningful CCM results for this model, is definitely beyond computational reach at this point. Secondly, our need is certainly less ambitious, since our ES results are only used here both to corroborate the intrinsically more accurate GS order parameter results, and to try to shed some more light on the nature of the states proximate to the quasiclassical AFM states under consideration.

We note again that the stability of the Néel-II phase that we have observed over a large parameter regime in the $\kappa\delta$ plane cannot be explained on classical grounds. Rather, for the case of a single layer (i.e., when $\delta = 0$), the Néel-II state exists for a certain range of values of κ for the spin- $\frac{1}{2}$ J_1 - J_2 model on the hexagonal lattice in which the classical model has spiral order. However, as is

generically always the case, quantum fluctuations tend to favor collinear order over non-collinear order. Hence, for the spin- $\frac{1}{2}$ J_1 - J_2 model, the collinear Néel-II state, which lies close in energy classically to the spiral ground state over a regime around $\kappa = \frac{1}{2}$, and which is actually degenerate in energy with the spiral states exactly at the classical critical point at $\kappa = \frac{1}{2}$, then becomes promoted by quantum fluctuation to be the lowest-energy state in a range of values around this point. This (rather fragile) stability of the AFM Néel-II phase is then initially enhanced, exactly as for the simpler AFM Néel state, by turning on an interlayer coupling, $\delta > 0$, in the spin- $\frac{1}{2}$ J_1 - J_2 - J_1^\perp model on the bilayer honeycomb lattice, when the ordering increases in both cases. The reason is presumably the same for both phases, and must again be a quantum effect, since at the classical level such an interlayer coupling plays no role whatsoever. Thus, for the spin- $\frac{1}{2}$ model a small interlayer coupling clearly enhances the AFM LRO of both quasiclassical (Néel and Néel-II) phases, as can clearly be seen from (Fig. 4 and) Fig. 8. However, as δ is increased further, any quasiclassical magnetic ordering in each layer now starts to compete with an IDVBC state formed as a product of interlayer singlet dimers between NN pairs on the *AA*-stacked bilayer. This increasing competition then leads ultimately, for both the Néel and Néel-II phases, to a weakening of their respective magnetic ordering, leading to the reentrant behavior seen clearly for both phases in Fig. 8. The reentrant effect is rather similar in both phases, with a maximum enhancement of the AFM magnetic LRO at a value $\delta \approx 0.2$, for the Néel case at an upper critical value $\kappa_1^{\max} \approx 0.215$ and for the Néel-II case at a lower critical value $\kappa_2^{\min} \approx 0.35$.

From our final results in Fig. 8 it is now easy to understand why accurate estimates for the positions of each of the two QCPs at $\kappa_c^{2,<}(0)$ and $\kappa_c^{2,>}(0)$, which delimit the range of values for the frustration parameter κ over which Néel-II magnetic LRO exists for the honeycomb-lattice monolayer, are so difficult to obtain. Thus, since the $\delta = 0$ axis is so close to the lower boundary $\delta = \delta_c^{2,<}(\kappa)$ of Néel-II stability in each monolayer, with the two layers coupled so that NN spins between them are antiparallel to one another, the inclusion of even a very small interlayer coupling is bound to have a much larger effect on the corresponding estimates for the QCPs. To a somewhat lesser extent, the same situation is also seen to be responsible for the sensitivity in estimating the (upper) critical point $\kappa_c^{1,>}(0)$ at which Néel order melts in the honeycomb-lattice monolayer.

While it is far beyond the scope of the present investigation to enquire in detail about the nature of the GS phases for the spin- $\frac{1}{2}$ J_1 - J_2 - J_1^\perp model on

the AA -stacked bilayer honeycomb lattice outside the regions shown in Fig. 8 where we have calculated that the model exhibits quasiclassical collinear AFM ordering of either the Néel or Néel-II type, we conclude with a few remarks on this issue. Firstly, our results for the ES parameter Δ , such as those shown in Figs. 5 and 6, clearly indicate the presence of a gapped paramagnetic state in part of the $\kappa\delta$ parameter space shown in Fig. 8. Broadly speaking, as indicated on the phase diagram, this gapped state exists over all (or most) of the region between the Néel and Néel-II islands of stability, as well as the region $\delta > \delta_c^{2,>}(\kappa)$ immediately above the Néel-II island of stability. There is also weak evidence from results such as those shown in Figs. 7(a) and 7(b) that this paramagnetic region also extends somewhat below the regions of stability of both the Néel and Néel-II phases, at least for values $\kappa \lesssim 1$. By contrast, results from calculations such as those shown in Figs. 5 and 7(c) indicate that at least part of the region below and to the right of the Néel-II island of stability is gapless. For reasons discussed more fully in Sec. 2, the gapped paramagnetic region is most likely to comprise VBC phases of different sorts, including those of the plaquette (PVBC) and staggered dimer (SDVBC) type on each monolayer and the interlayer dimer (IDVBC) type between the two layers. Similarly, the gapless state in the region indicated above is likely to be a quasiclassical state with spiral ordering. We hope that our preliminary findings concerning the possible regions of stability of the paramagnetic and spiral phases for the bilayer might inspire other calculations to investigate in more detail their regions of stability.

ACKNOWLEDGMENT

We thank the University of Minnesota Supercomputing Institute for the grant of supercomputing facilities, on which the work reported here was performed.

References

- [1] J. Richter, J. Schulenburg, A. Honecker, Quantum magnetism in two dimensions: From semi-classical Néel order to magnetic disorder, in: U. Schollwöck, J. Richter, D. J. J. Farnell, R. F. Bishop (Eds.), Quantum Magnetism, Lecture Notes in Physics Vol. 645, Springer-Verlag, Berlin, 2004, pp. 85–153.
URL <https://www.springer.com/gp/book/9783540214229>

- [2] D. J. J. Farnell, O. Götze, J. Richter, R. F. Bishop, P. H. Y. Li,
Quantum $s = \frac{1}{2}$ antiferromagnets on Archimedean lattices: The route from semiclassical mag
Phys. Rev. B 89 (2014) 184407. doi:10.1103/PhysRevB.89.184407.
URL <https://link.aps.org/doi/10.1103/PhysRevB.89.184407>
- [3] E. Rastelli, A. Tassi, L. Reatto, Non-simple magnetic order for simple Hamiltonians,
Physica B & C 97 (1) (1979) 1–24.
doi:10.1016/0378-4363(79)90002-0.
URL <http://www.sciencedirect.com/science/article/pii/0378436379900020>
- [4] A. Mattsson, P. Fröjdh, T. Einarsson,
Frustrated honeycomb Heisenberg antiferromagnet: A Schwinger-boson approach,
Phys. Rev. B 49 (1994) 3997–4002. doi:10.1103/PhysRevB.49.3997.
URL <https://link.aps.org/doi/10.1103/PhysRevB.49.3997>
- [5] J. B. Fouet, P. Sindzingre, C. Lhuillier,
An investigation of the quantum J_1 – J_2 – J_3 model on the honeycomb lattice,
Eur. Phys. J. B 20 (2) (2001) 241–254. doi:10.1007/s100510170273.
URL <https://doi.org/10.1007/s100510170273>
- [6] A. Mulder, R. Ganesh, L. Capriotti, A. Paramekanti,
Spiral order by disorder and lattice nematic order in a frustrated Heisenberg antiferromagnet
Phys. Rev. B 81 (2010) 214419. doi:10.1103/PhysRevB.81.214419.
URL <https://link.aps.org/doi/10.1103/PhysRevB.81.214419>
- [7] R. Ganesh, D. N. Sheng, Y.-J. Kim, A. Paramekanti,
Quantum paramagnetic ground states on the honeycomb lattice and field-induced Néel order
Phys. Rev. B 83 (2011) 144414. doi:10.1103/PhysRevB.83.144414.
URL <https://link.aps.org/doi/10.1103/PhysRevB.83.144414>
- [8] R. Ganesh, D. N. Sheng, Y.-J. Kim, A. Paramekanti,
Publisher’s Note: Quantum paramagnetic ground states on the honeycomb lattice and field-i
Phys. Rev. B 83 (2011) 219903(E). doi:10.1103/PhysRevB.83.219903.
URL <https://link.aps.org/doi/10.1103/PhysRevB.83.219903>
- [9] B. K. Clark, D. A. Abanin, S. L. Sondhi,
Nature of the spin liquid state of the Hubbard model on a honeycomb lattice,
Phys. Rev. Lett. 107 (2011) 087204.
doi:10.1103/PhysRevLett.107.087204.
URL <https://link.aps.org/doi/10.1103/PhysRevLett.107.087204>

- [10] J. Reuther, D. A. Abanin, R. Thomale,
Magnetic order and paramagnetic phases in the quantum J_1 - J_2 - J_3 honeycomb model,
Phys. Rev. B 84 (2011) 014417. doi:10.1103/PhysRevB.84.014417.
URL <https://link.aps.org/doi/10.1103/PhysRevB.84.014417>
- [11] A. F. Albuquerque, D. Schwandt, B. Hetényi,
S. Capponi, M. Mambrini, A. M. Läuchli,
Phase diagram of a frustrated quantum antiferromagnet on the honeycomb lattice: Magnetic
Phys. Rev. B 84 (2011) 024406. doi:10.1103/PhysRevB.84.024406.
URL <https://link.aps.org/doi/10.1103/PhysRevB.84.024406>
- [12] H. Mosadeq, F. Shahbazi, S. A. Jafari,
Plaquette valence bond ordering in a J_1 - J_2 Heisenberg antiferromagnet on a honeycomb lattice,
J. Phys.: Condens. Matter 23 (22) (2011) 226006.
doi:10.1088/0953-8984/23/22/226006.
URL <http://stacks.iop.org/0953-8984/23/i=22/a=226006>
- [13] J. Oitmaa, R. R. P. Singh, Phase diagram of the J_1 - J_2 - J_3 Heisenberg model on the honeycomb lattice,
Phys. Rev. B 84 (2011) 094424. doi:10.1103/PhysRevB.84.094424.
URL <https://link.aps.org/doi/10.1103/PhysRevB.84.094424>
- [14] F. Mezzacapo, M. Boninsegni, Ground-state phase diagram of the quantum J_1 - J_2 model on the honeycomb lattice,
Phys. Rev. B 85 (2012) 060402(R). doi:10.1103/PhysRevB.85.060402.
URL <https://link.aps.org/doi/10.1103/PhysRevB.85.060402>
- [15] P. H. Y. Li, R. F. Bishop, D. J. J. Farnell, C. E. Campbell,
Phase diagram of a frustrated Heisenberg antiferromagnet on the honeycomb lattice: The J_1 - J_2 model,
Phys. Rev. B 86 (2012) 144404. doi:10.1103/PhysRevB.86.144404.
URL <https://link.aps.org/doi/10.1103/PhysRevB.86.144404>
- [16] R. F. Bishop, P. H. Y. Li, D. J. J. Farnell, C. E. Campbell,
The frustrated Heisenberg antiferromagnet on the honeycomb lattice: J_1 - J_2 model,
J. Phys.: Condens. Matter 24 (23) (2012) 236002.
doi:10.1088/0953-8984/24/23/236002.
URL <http://stacks.iop.org/0953-8984/24/i=23/a=236002>
- [17] R. F. Bishop, P. H. Y. Li, C. E. Campbell,
Valence-bond crystalline order in the $s = 1/2$ J_1 - J_2 model on the honeycomb lattice,
J. Phys.: Condens. Matter 25 (30) (2013) 306002.

doi:10.1088/0953-8984/25/30/306002.

URL <http://stacks.iop.org/0953-8984/25/i=30/a=306002>

- [18] H. Zhang, C. A. Lamas, Exotic disordered phases in the quantum J_1 - J_2 model on the honeycomb lattice, Phys. Rev. B 87 (2013) 024415. doi:10.1103/PhysRevB.87.024415.
URL <https://link.aps.org/doi/10.1103/PhysRevB.87.024415>
- [19] R. Ganesh, J. van den Brink, S. Nishimoto, Deconfined criticality in the frustrated Heisenberg honeycomb antiferromagnet, Phys. Rev. Lett. 110 (2013) 127203. doi:10.1103/PhysRevLett.110.127203.
URL <https://link.aps.org/doi/10.1103/PhysRevLett.110.127203>
- [20] Z. Zhu, D. A. Huse, S. R. White, Weak plaquette valence bond order in the $S = 1/2$ honeycomb J_1 - J_2 Heisenberg model, Phys. Rev. Lett. 110 (2013) 127205. doi:10.1103/PhysRevLett.110.127205.
URL <https://link.aps.org/doi/10.1103/PhysRevLett.110.127205>
- [21] S.-S. Gong, D. N. Sheng, O. I. Motrunich, M. P. A. Fisher, Phase diagram of the spin- $\frac{1}{2}$ J_1 - J_2 Heisenberg model on a honeycomb lattice, Phys. Rev. B 88 (2013) 165138. doi:10.1103/PhysRevB.88.165138.
URL <https://link.aps.org/doi/10.1103/PhysRevB.88.165138>
- [22] X.-L. Yu, D.-Y. Liu, P. Li, L.-J. Zou, Ground-state and finite-temperature properties of spin liquid phase in the J_1 - J_2 honeycomb lattice, Physica E 59 (2014) 41–49. doi:10.1016/j.physe.2013.12.017.
URL <http://www.sciencedirect.com/science/article/pii/S1386947713004542>
- [23] R. Ganesh, S. V. Isakov, A. Paramekanti, Néel to dimer transition in spin- S antiferromagnets: Comparing bond operator theory with quantum Monte Carlo, Phys. Rev. B 84 (2011) 214412. doi:10.1103/PhysRevB.84.214412.
URL <https://link.aps.org/doi/10.1103/PhysRevB.84.214412>
- [24] H. Zhang, M. Arlego, C. A. Lamas, Quantum phases in the frustrated Heisenberg model on the bilayer honeycomb lattice, Phys. Rev. B 89 (2014) 024403. doi:10.1103/PhysRevB.89.024403.
URL <https://link.aps.org/doi/10.1103/PhysRevB.89.024403>
- [25] M. Arlego, C. A. Lamas, H. Zhang, Self consistent study of the quantum phases in a frustrated antiferromagnet on the bilayer honeycomb lattice, Phys. Rev. B 89 (2014) 024403. doi:10.1103/PhysRevB.89.024403.
URL <https://link.aps.org/doi/10.1103/PhysRevB.89.024403>

- J. Phys.: Conf. Ser. 568 (4) (2014) 042019.
doi:10.1088/1742-6596/568/4/042019.
URL <http://stacks.iop.org/1742-6596/568/i=4/a=042019>
- [26] R. F. Bishop, P. H. Y. Li, Frustrated honeycomb-bilayer Heisenberg antiferromagnet: The spin
Phys. Rev. B 95 (2017) 134414. doi:10.1103/PhysRevB.95.134414.
URL <https://link.aps.org/doi/10.1103/PhysRevB.95.134414>
- [27] P. H. Y. Li, R. F. Bishop, Transverse magnetic susceptibility of a frustrated spin- $\frac{1}{2}$ J_1 - J_2 - J_1^\perp H
AIP Conf. Proc. 1912 (1) (2017) 020011. doi:10.1063/1.5016136.
URL <https://aip.scitation.org/doi/abs/10.1063/1.5016136>
- [28] F. Coester, Bound states of a many-particle system, Nucl. Phys. 7
(1958) 421–424. doi:10.1016/0029-5582(58)90280-3.
URL <http://www.sciencedirect.com/science/article/pii/0029558258902803>
- [29] F. Coester, H. Kümmel, Short-range correlations in nuclear wave functions,
Nucl. Phys. 17 (1960) 477–485. doi:10.1016/0029-5582(60)90140-1.
URL <http://www.sciencedirect.com/science/article/pii/0029558260901401>
- [30] J. Čížek, On the correlation problem in atomic and molecular systems. Calculation of wavefun
J. Chem. Phys. 45 (11) (1966) 4256–4266. doi:10.1063/1.1727484.
URL <https://doi.org/10.1063/1.1727484>
- [31] H. Kümmel, K. H. Lührmann, J. G. Zabolitzky,
Many-fermion theory in $\exp S$ (or coupled cluster) form, Phys Rep.
36 (1) (1978) 1–63. doi:10.1016/0370-1573(78)90081-9.
URL <http://www.sciencedirect.com/science/article/pii/0370157378900819>
- [32] R. F. Bishop, K. H. Lührmann, Electron correlations: I. Ground-state results in the high-dens
Phys. Rev. B 17 (1978) 3757–3780. doi:10.1103/PhysRevB.17.3757.
URL <https://link.aps.org/doi/10.1103/PhysRevB.17.3757>
- [33] R. F. Bishop, K. H. Lührmann, Electron correlations. II. Ground-state results at low and meta
Phys. Rev. B 26 (1982) 5523–5557. doi:10.1103/PhysRevB.26.5523.
URL <https://link.aps.org/doi/10.1103/PhysRevB.26.5523>
- [34] J. Arponen, Variational principles and linked-cluster $\exp S$ expansions for static and dynamic
Ann. Phys. (N.Y.) 151 (2) (1983) 311–382.
doi:10.1016/0003-4916(83)90284-1.
URL <http://www.sciencedirect.com/science/article/pii/0003491683902841>

- [35] R. F. Bishop, H. G. Kmmel, The coupled-cluster method, *Phys. Today* 40(3) (1987) 52–60. doi:10.1063/1.881103.
- [36] J. S. Arponen, R. F. Bishop, E. Pajanne, Extended coupled-cluster method. I. Generalized coherent bosonization as a mapping of quantum magnetism, *Phys. Rev. A* 36 (1987) 2519–2538. doi:10.1103/PhysRevA.36.2519. URL <https://link.aps.org/doi/10.1103/PhysRevA.36.2519>
- [37] J. S. Arponen, R. F. Bishop, E. Pajanne, Extended coupled-cluster method. II. Excited states and generalized random-phase approximation, *Phys. Rev. A* 36 (1987) 2539–2549. doi:10.1103/PhysRevA.36.2539. URL <https://link.aps.org/doi/10.1103/PhysRevA.36.2539>
- [38] R. J. Bartlett, Coupled-cluster approach to molecular structure and spectra: A step toward practicality, *J. Phys. Chem.* 93 (5) (1989) 1697–1708. doi:10.1021/j100342a008. URL <https://doi.org/10.1021/j100342a008>
- [39] J. S. Arponen, R. F. Bishop, Independent-cluster parametrizations of wave functions in model systems, *Ann. Phys. (N.Y.)* 207 (1) (1991) 171–217. doi:10.1016/0003-4916(91)90183-9. URL <http://www.sciencedirect.com/science/article/pii/0003491691901839>
- [40] R. F. Bishop, An overview of coupled cluster theory and its applications in physics, *Theor. Chim. Acta* 80 (1991) 95–148. doi:10.1007/BF01119617.
- [41] R. F. Bishop, The coupled cluster method, in: J. Navarro, A. Polls (Eds.), *Microscopic Quantum Many-Body Theories and Their Applications*, Lecture Notes in Physics Vol. 510, Springer-Verlag, Berlin, 1998, pp. 1–70. doi:10.1007/BFb0104523.
- [42] C. Zeng, D. J. J. Farnell, R. F. Bishop, An efficient implementation of high-order coupled-cluster techniques applied to quantum magnetism, *J. Stat. Phys.* 90 (1) (1998) 327–361. doi:10.1023/A:1023220222019. URL <https://doi.org/10.1023/A:1023220222019>
- [43] D. J. J. Farnell, R. F. Bishop, The coupled cluster method applied to quantum magnetism, in: U. Schollwck, J. Richter, D. J. J. Farnell, R. F. Bishop (Eds.), *Quantum Magnetism*, Lecture Notes in Physics Vol. 645, Springer-Verlag, Berlin, 2004, pp. 307–348. doi:10.1007/BFb0119597.

- [44] D. J. J. Farnell, R. F. Bishop, P. H. Y. Li, J. Richter, C. E. Campbell,
Frustrated Heisenberg antiferromagnet on the honeycomb lattice: A candidate for deconfined
Phys. Rev. B 84 (2011) 012403. doi:10.1103/PhysRevB.84.012403.
URL <https://link.aps.org/doi/10.1103/PhysRevB.84.012403>
- [45] P. H. Y. Li, R. F. Bishop, D. J. J. Farnell, J. Richter, C. E. Campbell,
Ground-state phases of the frustrated spin- $\frac{1}{2}$ J_1 - J_2 - J_3 Heisenberg ferromagnet ($J_1 < 0$) on the
Phys. Rev. B 85 (2012) 085115. doi:10.1103/PhysRevB.85.085115.
URL <https://link.aps.org/doi/10.1103/PhysRevB.85.085115>
- [46] R. F. Bishop, P. H. Y. Li, Complete phase diagram of the spin- $\frac{1}{2}$ J_1 - J_2 - J_3 model (with $J_3 = J_1$)
Phys. Rev. B 85 (2012) 155135. doi:10.1103/PhysRevB.85.155135.
URL <https://link.aps.org/doi/10.1103/PhysRevB.85.155135>
- [47] R. F. Bishop, P. H. Y. Li, C. E. Campbell,
Frustrated spin- $\frac{1}{2}$ J_1 - J_2 isotropic XY model on the honeycomb lattice,
Phys. Rev. B 89 (2014) 214413. doi:10.1103/PhysRevB.89.214413.
URL <https://link.aps.org/doi/10.1103/PhysRevB.89.214413>
- [48] P. H. Y. Li, R. F. Bishop, C. E. Campbell,
Phase diagram of a frustrated spin- $\frac{1}{2}$ J_1 - J_2 XXZ model on the honeycomb lattice,
Phys. Rev. B 89 (2014) 220408(R). doi:10.1103/PhysRevB.89.220408.
URL <https://link.aps.org/doi/10.1103/PhysRevB.89.220408>
- [49] R. F. Bishop, P. H. Y. Li, C. E. Campbell,
Highly frustrated spin-lattice models of magnetism and their quantum phase transitions: A review
AIP Conf. Proc. 1619 (1) (2014) 40–50. doi:10.1063/1.4899216.
URL <https://aip.scitation.org/doi/abs/10.1063/1.4899216>
- [50] R. F. Bishop, P. H. Y. Li, O. Götze, J. Richter, C. E. Campbell,
Frustrated Heisenberg antiferromagnet on the honeycomb lattice: Spin gap and low-energy physics
Phys. Rev. B 92 (2015) 224434. doi:10.1103/PhysRevB.92.224434.
URL <https://link.aps.org/doi/10.1103/PhysRevB.92.224434>
- [51] R. F. Bishop, P. H. Y. Li, Large- s expansions for the low-energy parameters of the honeycomb lattice
J. Magn. Magn. Mater. 407 (2016) 348–357.
doi:10.1016/j.jmmm.2016.01.101.
URL <http://www.sciencedirect.com/science/article/pii/S0304885316301019>

- [52] P. H. Y. Li, R. F. Bishop, Ground-state phases of the spin-1 J_1 - J_2 Heisenberg antiferromagnet, Phys. Rev. B 93 (2016) 214438. doi:10.1103/PhysRevB.93.214438.
URL <https://link.aps.org/doi/10.1103/PhysRevB.93.214438>
- [53] P. H. Y. Li, R. F. Bishop, C. E. Campbell, Frustrated Heisenberg antiferromagnet on the honeycomb lattice with spin quantum number $S=1$, J. Phys.: Conf. Ser. 702 (1) (2016) 012001.
doi:10.1088/1742-6596/702/1/012001.
URL <http://stacks.iop.org/1742-6596/702/i=1/a=012001>
- [54] J. Villain, A magnetic analogue of stereoisomerism : Application to helimagnetism in two dimensions, J. Phys. (France) 38 (1977) 385–391.
doi:10.1051/jphys:01977003804038500.
URL <https://doi.org/10.1051/jphys:01977003804038500>
- [55] J. Villain, R. Bidaux, J.-P. Carton, R. Conte, Order as an effect of disorder, J. Phys. (France) 41 (11) (1980) 1263–1272. doi:10.1051/jphys:0198000410110126300.
URL <https://doi.org/10.1051/jphys:0198000410110126300>
- [56] E. F. Shender, Antiferromagnetic garnets with fluctuationally interacting sublattices, Zh. Eksp. Teor. Fiz. 83 (1982) 326–337.
URL <http://www.jetp.ac.ru/cgi-bin/e/index/r/83/1/p326?a=list>
- [57] R. J. Bartlett, M. Musiał, Coupled-cluster theory in quantum chemistry, Rev. Mod. Phys. 79 (2007) 291–352. doi:10.1103/RevModPhys.79.291.
URL <https://link.aps.org/doi/10.1103/RevModPhys.79.291>
- [58] We use the program package CCCM of D. J. J. Farnell and J. Schulenburg, see <http://www-e.uni-magdeburg.de/jschulen/ccm/index.html>.
[link].
URL <http://www-e.uni-magdeburg.de/jschulen/ccm/index.html>
- [59] P. H. Y. Li, R. F. Bishop, Gapped paramagnetic state in a frustrated spin- $\frac{1}{2}$ Heisenberg antiferromagnet, J. Magn. Magn. Mater. 449 (2018) 127–132.
doi:10.1016/j.jmmm.2017.09.078.
URL <http://www.sciencedirect.com/science/article/pii/S030488531732200X>
- [60] S. E. Krüger, J. Richter, J. Schulenburg, D. J. J. Farnell, R. F. Bishop, Quantum phase transitions of a square-lattice Heisenberg antiferromagnet with two kinds of interactions, Phys. Rev. B 97 (2018) 104407. doi:10.1103/PhysRevB.97.104407.
URL <https://link.aps.org/doi/10.1103/PhysRevB.97.104407>

- Phys. Rev. B 61 (2000) 14607–14615.
doi:10.1103/PhysRevB.61.14607.
URL <https://link.aps.org/doi/10.1103/PhysRevB.61.14607>
- [61] J. Richter, R. Zinke, D. J. J. Farnell,
The spin-1/2 square-lattice J_1 – J_2 model: the spin-gap issue, Eur.
Phys. J. B 88 (2015) 2. doi:10.1140/epjb/e2014-50589-x.
URL <https://doi-org.manchester.idm.oclc.org/10.1140/epjb/e2014-50589-x>
- [62] R. F. Bishop, P. H. Y. Li, Spin-gap study of the spin- $\frac{1}{2}$ J_1 – J_2 model on the triangular lattice,
EPL 112 (6) (2015) 67002. doi:10.1209/0295-5075/112/67002.
URL <http://stacks.iop.org/0295-5075/112/i=6/a=67002>
- [63] R. F. Bishop, P. H. Y. Li, High-order study of the quantum critical behavior of a frustrated sp
Phys. Rev. B 96 (2017) 224416. doi:10.1103/PhysRevB.96.224416.
URL <https://link.aps.org/doi/10.1103/PhysRevB.96.224416>